On the Quasi-Static Perforation Resistance of Circular AA5083-H116 Aluminium Plates

F. Grytten[1], T. Børvik[1,2], O.S. Hopperstad[1] and M. Langseth[1]

[1]*Structural Impact Laboratory (SIMLab), Department of Structural Engineering*
Norwegian University of Science and Technology
NO-7491, Trondheim, Norway

[2]*Research and Development Department*
Norwegian Defence Estates Agency
NO-0103, Oslo, Norway

E-mail: frode.grytten@ntnu.no

Abstract

This paper presents numerical simulations of quasi-static perforation of circular AA5083-H116 aluminium plates. The perforation process was analysed with 2D-axisymmetric elements, brick elements and shell elements. Slightly modified versions of the Johnson-Cook constitutive relation and fracture criterion were used in the finite element simulations to model the material behaviour. A factorial design was used to investigate the influence of varying plate thickness, boundary conditions, punch diameter and nose shape. Comparisons between LS-DYNA simulations and experiments were made and good qualitative agreement was in general found. However, some quantitative differences were observed.

Key words: Modified Johnson-Cook models, fracture.

Introduction

Perforation of plates is considered as a complex process, involving among other factors large strains, contact, damage and fracture. Thus, research in this field has generally been of an empirical nature. The increase in computer performance over the last decades has, however, made finite element analysis more available to this type of problems. Engineers have started to optimize designs using finite element models and it seems to be a general opinion that the understanding of the physical processes during perforation can increase through validated numerical simulations. It is therefore of crucial importance that the numerical models are validated through comparison with experiments, especially when new materials are introduced.

AA5083-H116 is among the strongest commercial aluminium-magnesium alloys available, and is well suited for rolling. Since the alloy also has good corrosion resistance, it is often used in plates in offshore structures where accidental loading from dropped objects may be a concern.

Experiments

The quasi-static experiments were carried out in a test rig where a replaceable punch was connected to a hydraulic actuator. A circular rigid frame was used as a support for the plates, giving a free span diameter of 500 mm. The load was applied at a constant displacement rate of 3 mm/min. Punch displacement and interface force were continuously measured during the tests. In some of the tests the out-of-plane displacement of the entire plate was measured optically and contour maps of the plate deformation at different load levels were made.

The target thickness, punch nose shape, punch diameter and the boundary conditions of the target plate were changed according to a factorial design. The effect on the maximum force the plates could resist before fracture and the energy required to perforate the plates were studied. Plates with thickness 3, 5 and 10 mm were perforated with blunt and hemispherical punches with diameters of 20 and 30 mm. The boundary conditions of the plates were either clamped or simply supported. Plugging failure was observed in all experiments with blunt nose shape, while petaling was observed in most of the experiments with hemispherical nose shape. A combination of plug formation and petaling was observed in the remaining experiments with hemispherical nose. Figure 1 shows sketches of the observed fracture modes.

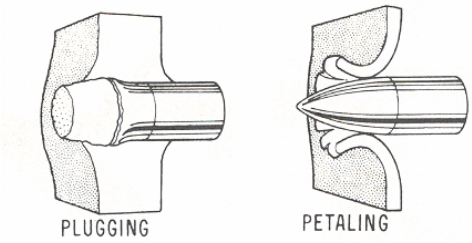

Figure 1 Failure modes in plate impact [11]

In addition, the effect of changing target thickness, punch diameter and boundary condition on the displacement at maximum force and on the energy required to perforate the plate was investigated for the plates perforated with a blunt punch.

Results from tests will be compared with results from LS-DYNA [5] simulations later on in this paper.

Material model

The perforation process has been simulated with axisymmetric elements, brick elements and shell elements. Slightly modified versions of the two Johnson-Cook models describing flow stress [6] and fracture [7], as proposed by Børvik et al. [2] and implemented in LS-DYNA [5] as *MAT_107, were used in all finite element models. The constitutive relation reads

$$\sigma_{eq} = \left(A + B\varepsilon_{eq}^{n}\right)\left(1 + \dot{\varepsilon}_{eq}^{*}\right)^{C}\left(1 - T^{*m}\right) \tag{1}$$

where $\dot{\varepsilon}_{eq}^{*} = \dot{\varepsilon}_{eq}/\dot{\varepsilon}_{0}$ is a dimensionless plastic strain rate, $\dot{\varepsilon}_{0}$ is a reference strain rate, ε_{eq} is the equivalent plastic strain and σ_{eq} is the von Mises equivalent stress. $\mathrm{T}^{*} = \left(\mathrm{T} - \mathrm{T}_{0}\right)/\left(\mathrm{T}_{\mathrm{m}} - \mathrm{T}_{0}\right)$ is

the homologous temperature, T_0 is room temperature and T_m is the melting temperature, and A, B, n, C and m are material constants. Assuming adiabatic conditions the rate of temperature is often defined as

$$\dot{T} \approx \chi \frac{\sigma_{eq}\dot{\varepsilon}_{eq}}{\rho C_p} \tag{2}$$

where χ is the Taylor-Quinney empirical constant, ρ is the density and C_p is the specific heat capacity at constant pressure.

The modified Johnson-Cook failure criterion proposed by Børvik et al. [2] reads

$$D = \sum \frac{\Delta\varepsilon_{eq}}{\varepsilon_f} \leq 1 \tag{3}$$

$$\varepsilon_f = \left(D_1 + D_2 e^{D_3\sigma^*}\right)\left(1+\dot{\varepsilon}_{eq}^*\right)^{D_4}\left(1+D_5 T^*\right) \tag{4}$$

where D_1, D_2, D_3, D_4 and D_5 are material constants. Equation (4) relates the fracture strain to the stress triaxiality ratio given as

$$\sigma^* = \frac{\sigma_m}{\sigma_{eq}} \tag{5}$$

and to the strain rate and the temperature. When the damage parameter D reaches unity, fracture is assumed to occur.

It is assumed that temperature effects play a minor role in quasi-static penetrations [9]. The parameters χ and D_5 are therefore set equal to zero in the present study.

The hardening parameters A, B and n were found from uniaxial tensile tests. A device that can measure the cross sectional area was used during the tests as described by Børvik et al. [2]. Thus, the true average stress could be found all the way to fracture. By assuming plastic incompressibility the corresponding true plastic strain was obtained. In this way the true stress-strain curve was found until fracture in uniaxial tension, which corresponds to a stress triaxiality of $1/3$ before diffuse necking. Even so, extrapolation of the results is still required since the failure strain at lower triaxialities can be much greater. Some difference in the yield stress was found between the 3 mm thick plates and the two thicker plates. The same hardening parameters were used for both 5 and 10 mm since no apparent differences were seen. It is assumed that the observed difference in yield stress is caused by different degrees of work hardening in the cold rolling process.

Table 1 Hardening parameters

Plate thickness	A [MPa]	B [MPa]	n
5 mm & 10 mm	206	423	0.362
3 mm	223	423	0.441

Figure 2 shows the measured stress-strain curves compared to the fitted curve for the 3 mm thick material. The serrations seen in the plot are caused by strain-rate localizations, commonly known as the Portevin-Le Chatelier (PLC) effect. It is also noted that the material exhibits decreasing flow stress when the steady-state strain rate is increased in the range 10^{-5}-10^{2} s^{-1}. The Johnson-Cook model is not capable of describing the negative strain rate sensitivity mentioned above, but a promising model has been proposed by Zhang et al. [10]. However, as proposed by Clausen et al. [3] the reference strain rate was set to 1 s^{-1} and C was taken to be 0.001.

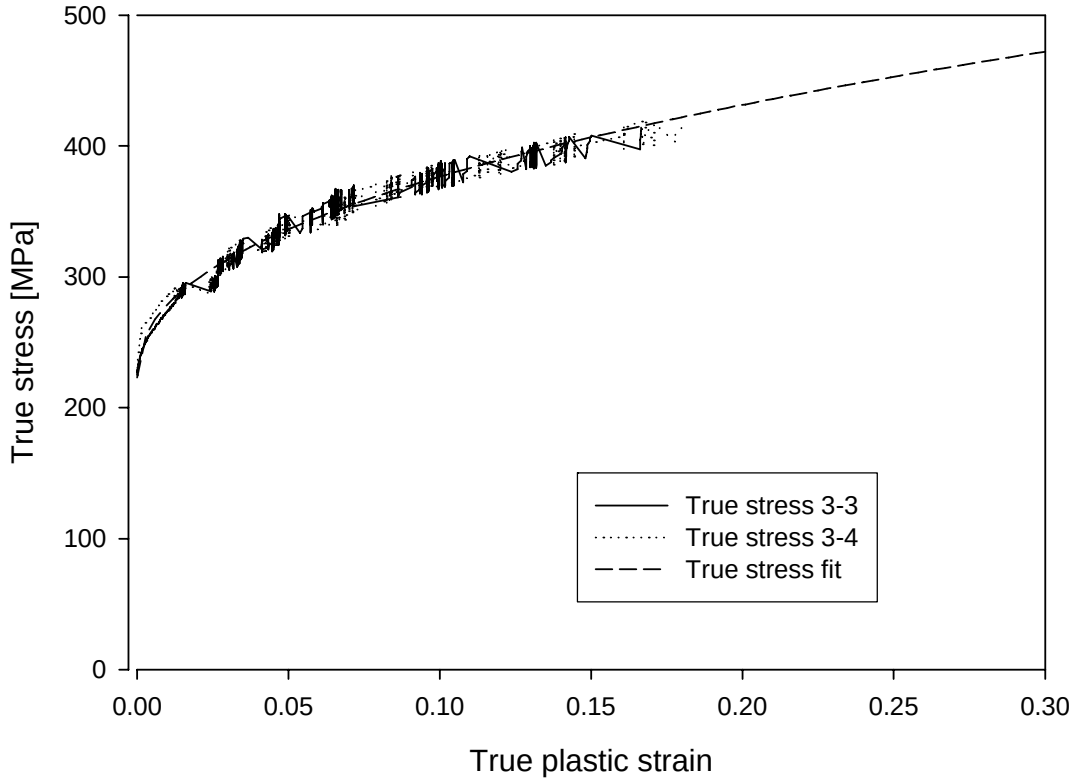

Figure 2 Measured true stress versus true plastic strain compared to fitted curve for 3 mm plate

The fracture parameters D_1, D_2 and D_3 were found by using a least square fit to data obtained by Clausen et al. [3]. Only the fracture strains measured in the microscope were used since those are regarded as the most accurate. All the measurements of Clausen et al. [3] are for positive triaxialities, thus an extrapolation into the negative range is necessary. As pointed out by Bao and Wierzbicki [1], this is risky and can lead to substantial errors. Bao and Wierzbicki [1] also claimed to have found from upsetting tests that fracture can never occur for triaxialities below $-1/3$. However, it is not possible to define a cut-off at $\sigma^* = -1/3$ with the Johnson-Cook failure criterion [7]. In order to prevent premature fracture in the compressed parts of the structure, the failure strain at negative stress triaxialities can be set significantly higher than the failure strains

observed for positive stress triaxialities. The failure strain at $\sigma^* = -1/3$ was therefore set equal to 1 in this study. This additional constraint to the curve fitting has proven to give sufficiently large failure strains for negative stress triaxialities without affecting the curve fit in the positive region too much. Anisotropy was neglected and the fracture parameters found were used for all plate thicknesses. The parameter D_4 governs the effect of strain rate and was taken from Clausen et al. [3]. The fracture parameters are given in Table 2. The curve obtained with these damage parameters is plotted together with the measured points in Figure 3.

Table 2 Fracture parameters

D_1	D_2	D_3	D_4	D_5
0.178	0.389	-2.25	0.147	0.00

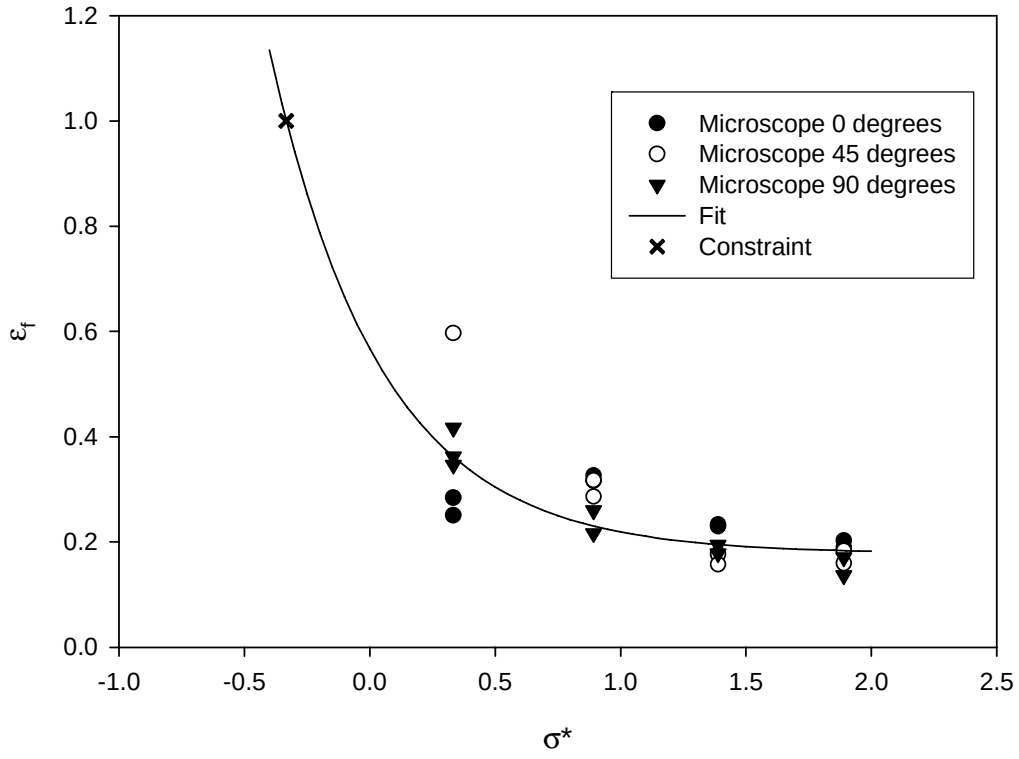

Figure 3 Failure strain as function of stress triaxiality ratio

Finite element simulations

When modelling the plate with axisymmetric elements, a characteristic element size of approximately 0.15 mm was chosen in the local region of the plate, defined as 1.2 times the diameter of the punch or projectile. The element size was doubled in the global part of the plate.

All the axisymmetric models failed by plugging, since radial cracking and petaling are not possible when axisymmetry is assumed. Axisymmetry also led to extensive element erosion. Even so, the behaviour until fracture initiation was well described and therefore the maximum

forces obtained with axisymmetric models agree well with the ones obtained in experiments and brick and shell element simulations. The axisymmetric simulations took from 7 to 20 hours to complete with a 3 GHz Intel Pentium 4 processor.

When using 8 node constant stress brick elements, the characteristic element size used was in the range 0.4 – 1 mm. A relatively good correlation was observed between the maximum force found with brick elements and the maximum force observed in experiments. However, the global response obtained with brick elements seems to be too stiff. This is probably caused by a too coarse mesh. The fracture modes observed in these finite element models correspond well to the fracture modes observed in the experiments. All plates loaded by a blunt-nosed punch failed by plugging as in the experiments. Furthermore, some of the plates loaded by a hemispherical nosed punch failed by petaling and some by plugging. The simulations with brick elements took typically around 40 hours to run.

In addition to modelling the penetration process with brick and axisymmetric elements, it was also modelled with Belytschko-Tsay shell elements. Ten integration points were used through the plate thickness in the local part, while 4 integration points were used in the rest of the plate. The shell element models were able to describe both plugging and petaling. Plugging is normally caused by transverse shear, and it was therefore not evident that the shell model should be capable of describing this. However, it seems like plugging is partly caused by tension on the rear side of the plate in these cases of quasi-static penetration of thin plates and this is probably the reason for why it worked after all. A typical simulation required 3 hours of CPU time.

Figure 4 shows the effects of varying target thickness, boundary conditions, punch nose shape and punch diameter on the maximum force found from experiments and axisymmetric simulations. The results obtained with brick and shell models are very close to the results obtained with axisymmetric elements. A relatively good correlation is observed. It can be seen that target thickness is the most important factor for the maximum force the target can take before fracture occurs. The boundary conditions have a negligible influence on the maximum force while the shape and diameter of the punch nose have a small effect. All this is seen in both experiments and simulations.

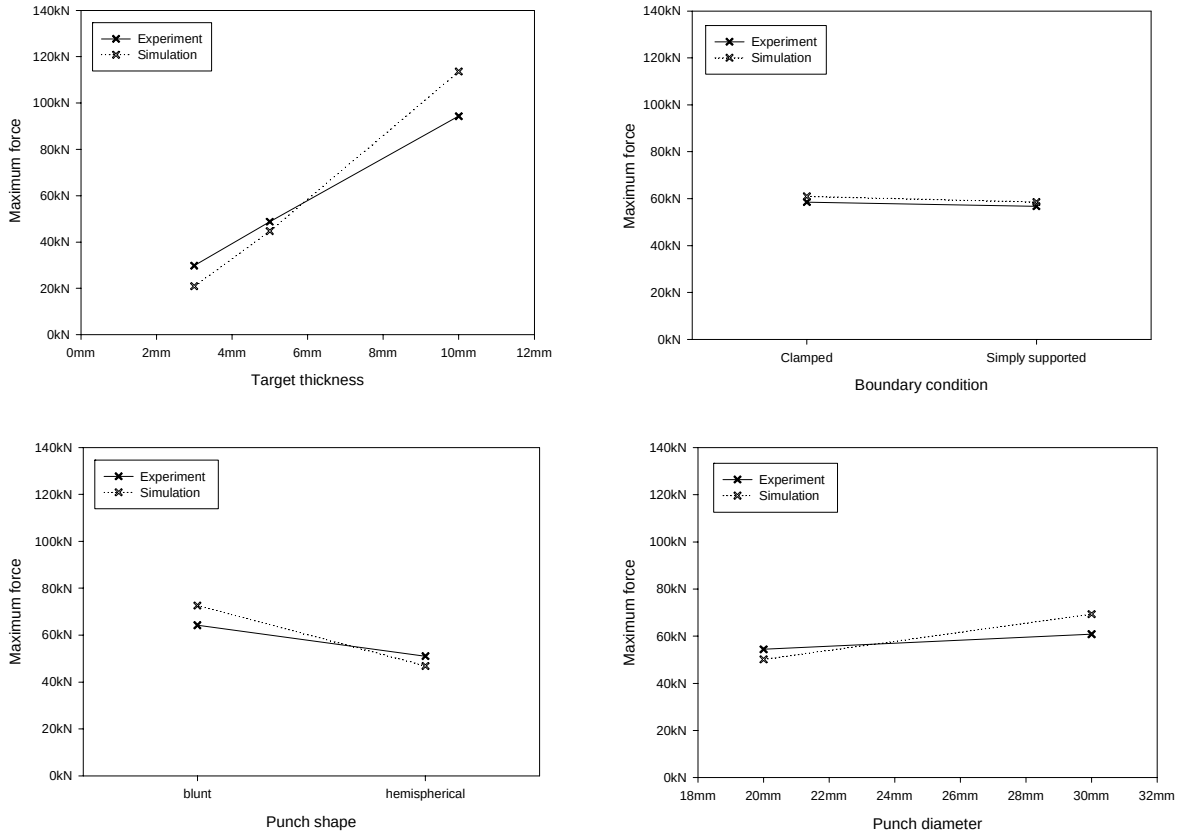

Figure 4 Comparison of effects on maximum force from experiments and axisymmetric simulations

The effect of changing target thickness, boundary condition and punch diameter on the maximum force, displacement at maximum force and the energy required to perforate the target was investigated only for the blunt nosed punches. Figure 5 shows a comparison of the effect found from experiments and axisymmetric simulations. Some discrepancies are observed, but the correlation between experiments and simulations is acceptable. The results obtained with shell elements correlated well with the results obtained with axisymmetric elements, while the brick element solutions seemed to be too stiff and therefore gave too small displacements and energies.

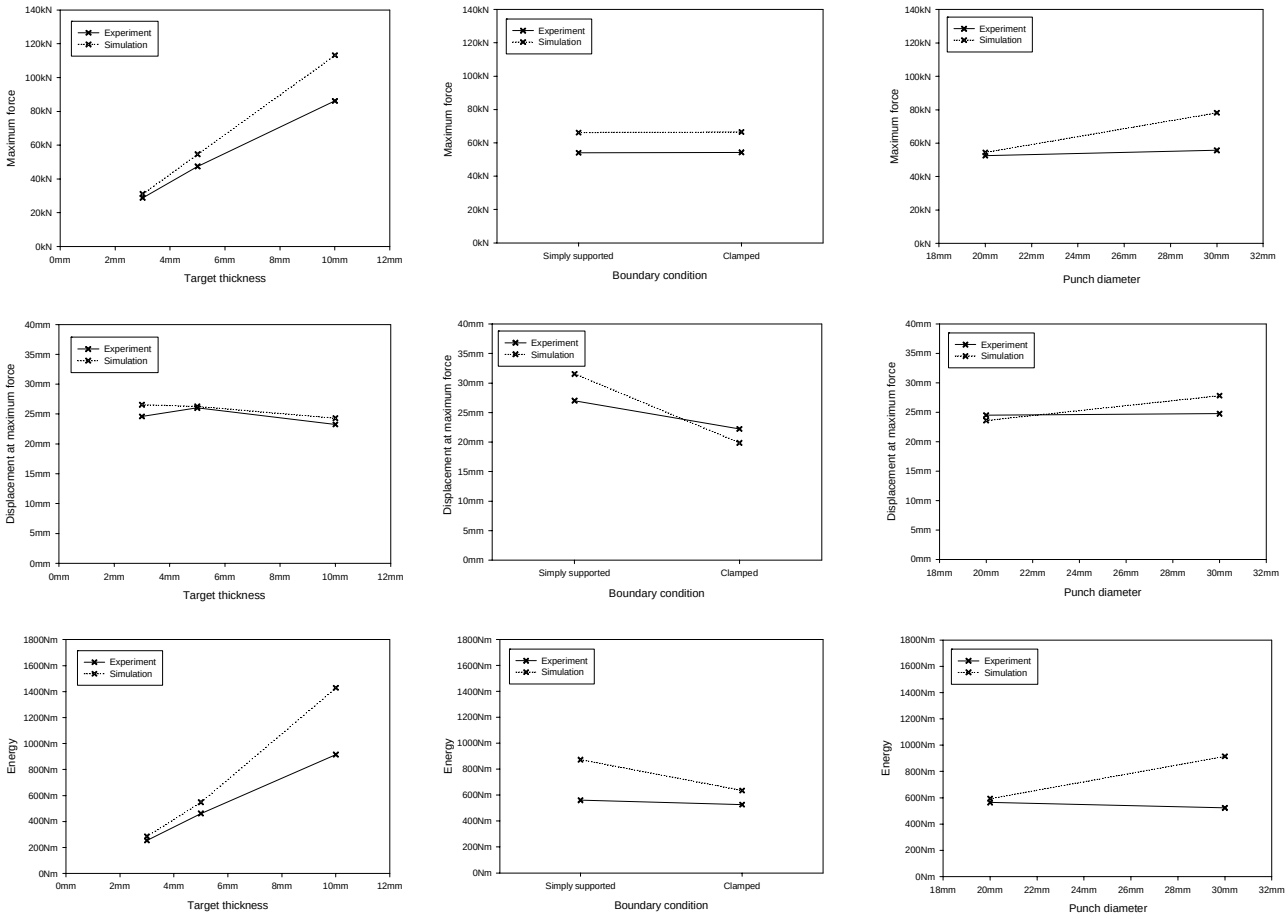

Figure 5 Comparison of effects with blunt punch from experiments and simulations

Conclusions

All the finite element models described in the previous section were able to predict the behaviour of the plate until fracture, and to predict the maximum force relatively well. Although the finite element models may differ from the experiments quantitatively, they seem to describe the penetration process qualitatively correct. The exception is the axisymmetric models which are not capable of describing radial cracks and petaling correctly. The effects of anisotropy and PLC effect are currently being investigated in an ongoing study.

References

[1] Bao, Y. and Wierzbicki, T. (2005), "On the cut-off value of negative triaxiality for fracture", Engineering Fracture Mechanics, vol 72, 1049-1069.

[2] Børvik, T., Hopperstad, O.S., Berstad, T. and Langseth, M. (2001), "A computational model of viscoplasticity and ductile damage for impact and penetration", Eur. J. Mech. A/Solids, vol 20, 685-712.

[3] Clausen, A. H., Børvik, T., Hopperstad, O.S. and Benallal, A. (2004). "Flow and fracture characteristics of aluminium alloy AA5083-H116 as function of strain rate, temperature and triaxiality", Materials Science and Engineering A, vol 364, 260-272.

[4] Fagerholdt, E., Grytten, F., Førre, B. and Børvik, T. (in progress), ”Out-of-plane deformation measurements of 5083-H116 aluminium plates during quasi-static perforation using structured light and close-range photogrammetry”.

[5] Hallquist, J. O. (1998), “LS-DYNA theoretical manual”, Livermore Software Technology Corporation.

[6] Johnson, G.R. and Cook, W.H. (1983), “A constitutive model and data for metals subjected to large strains, high strain rates and high temperatures”, in: Proceedings of Seventh International Symposium on Ballistics, The Hague.

[7] Johnson, G.R. and Cook, W.H. (1985), “Fracture characteristics of three metals subjected to various strains, strain rates, temperature and pressures”, Engineering Fracture Mechanics, vol 21, 31-48.

[8] Langseth, M. and Larsen, PK. (1990),“Dropped objects’ plugging capacity of steel plates: An experimental investigation”, Engineering Fracture Mechanics, vol 9, 289-316.

[9] Lindholm, U.S. and Johnson, G.R. (1983), “Strain-rate effects in metals at large shear strains”, in: Proceedings of the 29th Sagmore Army Materials Conference, Lake Placid, New York.

[10] Zhang, S., McCormick, P.G. and Estrin, Y. (2001), “The morphology of Portevin-Le Chatelier bands: Finite element simulation for Al-Mg-Si”, Acta Materialia, vol 49, 1087-1094.

[11] Zukas, J.A. (1982), “Penetration and perforation of solids” in: Zukas, J.A., Nicholas, T., Swift, H.F., Grezczuk, L.B. and Curran, D.R. (eds.) Impact Dynamics, John Wiley and Sons, Inc., New York, 155-214.